Physical and Microwave Radiative Properties of Precipitating Clouds. Part I: Principal Component Analysis of Observed Multichannel Microwave Radiances in Tropical Stratiform Rainfall

GRANT W. PETTY

Atmospheric and Oceanic Sciences, University of Wisconsin—Madison, Madison, Wisconsin

(Manuscript received 7 August 2000, in final form 18 June 2001)

ABSTRACT

Using stringent criteria pertaining to rain-cloud optical thickness and horizontal extent, 3203 multichannel microwave observations of heavy, widespread tropical precipitation over ocean were selected from 9 months of global Special Sensor Microwave Imager (SSM/I) data. These observations subsequently were found to be associated almost exclusively with stratiform rain areas in tropical cyclones. Because of the restrictions on optical thickness and spatial extent, the mean multichannel microwave brightness temperatures and their interchannel covariances are presumed to be determined primarily by the vertical microphysical structure of the rain clouds. The distribution of the above observations in seven-dimensional channel space is characterized concisely using principal component analysis. It is found that only three independent variables are sufficient to explain 97% of the variance in the correlation matrix. This result suggests that the radiometrically important microphysical properties of these rain clouds are strongly interdependent. The most significant eigenvector of the observation correlation matrix corresponds to variable scattering at high frequencies by ice aloft. Its spectral dependence is accurately given by $\nu^{1.76}$, where ν is the microwave frequency. This empirical result constrains the effective mean sizes of ice particles responsible for observed passive microwave scattering in rain clouds and provides a plausible empirical basis for accurately predicting the magnitude of scattering effects by ice at non-SSM/I microwave frequencies. There are also qualitative indications that this mode of brightness temperature variability is poorly correlated with surface rain rate in this study sample. The empirical results presented herein are expected to be of value for the validation and improvement of microphysical assumptions and optical parameterizations in forward microwave radiative transfer models. Companion papers describe the actual retrieval of effective rain-cloud microphysical properties from the observed multichannel radiances.

1. Introduction

The performance of physical model-based multichannel algorithms for the passive microwave retrieval of surface rain rate (Olson 1989; Wilheit et al. 1991; Bauer and Schluessel 1993; Petty 1994b; Aonashi et al. 1996; Wentz and Spencer 1998) and/or hydrometeor profiles (Smith et al. 1994; Evans et al. 1995; Kummerow et al. 1996; Marzano et al. 1995, 1999) depends in part on accurate forward models for the spectral and polarization dependence of cloud-top radiances on rain-cloud properties. The accuracy of any forward model, in turn, depends critically on all three of the following factors:

1) realism in the specification of hydrometeor sizes, shapes, and phases encountered in real rain clouds and their three-dimensional distribution;
2) the accurate specification of local optical properties (e.g., phase function, single scatter albedo, and volume extinction coefficient) from knowledge of the above hydrometeor properties; and
3) the accuracy and generality of the radiative transfer code itself.

Errors or inappropriate approximations at any one of these three stages can lead to inconsistencies between predicted and observed multichannel signatures (Panegrossi et al. 1998). Such inconsistencies in forward models can, in turn, lead to incorrect rain-rate or hydrometeor-profile retrievals or, at best, a reduction in the usable information content of the multichannel observations.

There has recently been considerable progress in the development of nonplane-parallel and/or polarized radiative transfer codes and in the accommodation by some models of nonspherical particles (Kummerow and Weinman 1988; Petty 1994b; Roberti et al. 1994; Evans and Stephens 1995a; Liu et al. 1996; Haferman et al. 1997; Roberti and Kummerow 1999). These improvements unfortunately, only address the third item and, to a limited extent, the second item in the above list. There

Corresponding author address: Grant W. Petty, Dept. of Atmospheric and Oceanic Sciences, University of Wisconsin—Madison, 1225 West Dayton St., Madison, WI 53706.
E-mail: gpetty@aos.wisc.edu

are globally still far too few direct observations of the relevant hydrometeor properties (and their statistical variability) in various types of rain clouds. Even when the hydrometeor properties themselves are thought to be reasonably well known, the validity of common parameterizations of the microwave optical properties of, say, highly irregular and/or loosely aggregated snow flakes remains very much in doubt.

Variability in the *N*-channel (vector) observations of rain clouds by a microwave radiometer in space must be due to variability in the properties of the rain clouds themselves. Observations from a sufficiently large sample may be thought of as describing an *N*-dimensional volume (or manifold) in channel space. If forward model calculations yield a radiance vector falling outside the observation manifold, then this lack of agreement signals either that the model itself is flawed or else that specific environmental parameters (e.g., particle size, cloud depth) assumed in the forward model are statistically unrepresentative of the rain clouds from which the observations were derived. The spectral and polarization dependence of the disagreement may offer clues as to how the model assumptions can be adjusted to improve agreement.

Even if a model calculation falls inside the manifold defined by the observations, one can still not assert that the model is correct, only that it is not demonstrably in error. Nevertheless, even that modest improvement in confidence may be beneficial, especially if the requirement for physical consistency with actual observations significantly tightens the range of uncertainty on those model parameters whose values were previously speculative.

The objectives of this multipart study are thus fourfold: 1) to document the actual satellite microwave multichannel radiances and their joint variability, associated with certain reasonably well-defined classes of precipitation; 2) to evaluate critically and, where appropriate, to revise key assumptions about actual rain-cloud microphysical properties as they relate to microwave radiative transfer; 3) to develop improved models and parameterizations of the interaction between microwave radiation and rain-cloud constituents; and 4) to assess the usable physical information content of multichannel microwave observations of real precipitation in view of the inherent variability or uncertainty of key rain-cloud properties.

This paper addresses the first objective above in the case of tropical oceanic rainfall observed by the Special Sensor Microwave Imager (SSM/I) and meeting minimum criteria for horizontal extent and optical depth. The data selection criteria employed herein are designed to reduce the role of surface emission and footprint filling in the observed brightness temperatures, leaving the microphysical structure of the rain clouds themselves as the foremost factor determining observed brightness temperatures.

Companion papers (Petty 2001; Petty and Gautam 2001, manuscript submitted to *J. Appl. Meteor.*, hereinafter PG01) address the problem of physically interpreting the observed SSM/I multichannel radiances described herein and of finding cloud model parameters that lead to consistency between those observed radiances and the calculated values from a radiative transfer model.

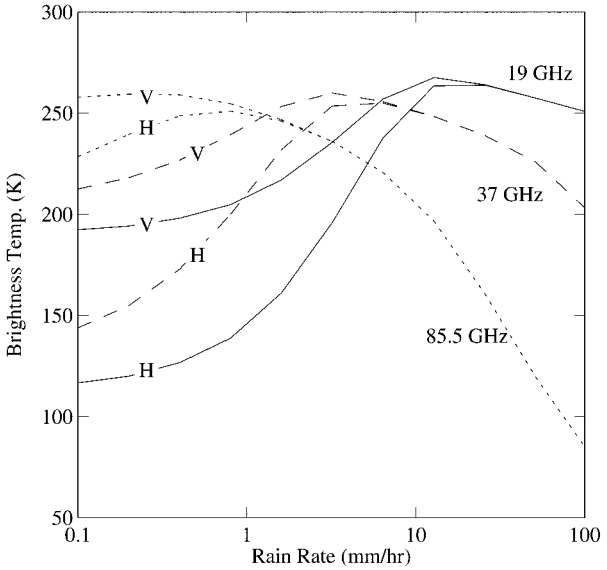

FIG. 1. Idealized brightness temperature dependence on surface rain rate.

2. SSM/I data

a. Instrument description

The SSM/I is a conically scanned radiometer that observes brightness temperatures at 19.35, 22.235, 37.0, and 85.5 GHz, in both vertical and horizontal polarizations (vertical-only for 22.235 GHz). The viewing incidence angle is 53° from vertical. The spatial resolution of SSM/I varies from 43 km × 69 km at 19.35 GHz to 13 km × 15 km at 85.5 GHz. The swath of SSM/I is about 1400 km. A detailed description of SSM/I can be found in Hollinger et al. (1990).

b. Response to precipitation

The ideal behavior of SSM/I brightness temperatures in response to horizontally uniform rain over the ocean is illustrated in Fig. 1. The behavior is similar for all frequencies except that the peak brightness temperature T_B and the loss of the polarization contribution from the ocean surface occur at progressively lower values of the surface rain rate R as the frequency increases. It must be emphasized that these curves represent idealizations and that the actual relationship between T_B and R depends also on a number of other factors such as background humidity, sea surface roughness, and so on

(Wentz 1992; Petty 1994b), as well as the microphysical properties of the rain cloud itself.

Over the open ocean, T_Bs observed by SSM/I are cold (approximately 100–240 K, depending on channel) and are strongly polarized, with typical differences between vertical and horizontal polarization being 20–70 K. To varying degrees, water vapor, cloud water, and precipitation in the atmosphere are capable of increasing the optical thickness of the atmosphere, which in turn tends to increase observed brightness temperatures while reducing the transmission of the polarized sea surface emission. However, at SSM/I frequencies, precipitation is the only atmospheric constituent that is capable of producing optical thicknesses that greatly exceed unity. When scattering is present, it has the effect of depressing brightness temperatures relative to those expected without scattering. Scattering typically becomes more important as rainfall intensity increases, so that brightness temperature increases with increasing rain intensity up to some maximum value, after which it decreases.

In addition to the information contained in the absolute T_B, there is information in the difference ΔT_B between vertically and horizontally polarized brightness temperatures at a given frequency, because this difference is largely a function of the visibility of the polarized emission of ocean surface through and between rain clouds. Among other things, polarization information may be used to eliminate the ambiguity associated with cold brightness temperatures, which may be due either to polarized emission from the unobscured ocean surface or to nearly unpolarized scattering from frozen precipitation aloft. See Petty (1994a) for a more detailed discussion of the interpretation of polarization information from passive microwave imagers.

The details of the T_B–R curves in Fig. 1, such as the position and height of the peak and the magnitude of the T_B depression in the scattering regime to the right of the peak, all depend strongly on the concentration, size, and density of ice particles aloft accompanying a given surface rain rate. Also, in contrast to the idealized case depicted in Fig. 1, the polarization difference at a given frequency may not vanish as the rain cloud becomes optically thick. Rather, scattering by both rain drops and ice particles viewed at an oblique angle can give rise to modest residual polarization differences. Differences of up to 2–3 K may be explained by spherical particles alone (Liu and Simmer 1996); observed differences of up to 10 K or more that are frequently observed in stratiform rain clouds (Spencer et al. 1989; Heymsfield and Fulton 1994) may depend on the presence of preferentially oriented nonspherical particles (Wu and Weinman 1984; Turk and Vivekanandan 1995; Evans and Stephens 1995b).

Note that the ideal response of SSM/I to rainfall as depicted in Fig. 1 assumes that the field of view (FOV) is completely filled with rain of uniform intensity. Given the coarse resolution of the SSM/I (see above), this assumption is difficult to satisfy in practice. The radiative consequences of rain-cloud inhomogeneity within the FOV can be broken down into three components: 1) the effects of averaging a nonlinear function of surface rain rate (e.g., the T_B–R relationships in Fig. 1) over the two-dimensional FOV—this is the classic ''beam-filling'' problem described by, for example, Wilheit (1986); 2) the effects of 3D geometry on the physical transfer of microwave radiation through a rain cloud—for example, ''leakage'' of upwelling thermal radiation out of the sides of a vertically developed cloud (Kummerow and Weinman 1988; Roberti et al. 1994; Liu et al. 1996; Haferman et al. 1997); and 3) the geometric effects occasioned by viewing three-dimensional structures at an oblique angle (53° from nadir for SSM/I) over a reflective surface, which leads to significant contributions from both the sides and the surface reflections of vertically developed clouds to the observed radiances (Petty 1994a; Liu et al. 1996). Inasmuch as the actual 3D structure of a rain cloud observed by satellite is rarely known in any given case, all of these effects, and particularly 1 and 3, are important sources of ambiguity in the physical interpretation of microwave T_B, whether for the estimation of surface rainfall or the inference of microphysical properties.

Because the objective of this paper is to isolate and to interpret something approximating the ''pure'' microwave signature of rainfall—that is, brightness temperatures that can be reasonably compared with the output of plane-parallel radiative transfer models without regard to surface variables and other extraneous influences—the next section describes the procedure for identifying SSM/I observations of rainfall which is 1) heavy and therefore nearly opaque even at 19.35 GHz and is 2) spatially extensive and therefore less susceptible to brightness temperature variations due to beam-filling and 3D geometric effects.

c. Sample selection

For the 9-month period of April–December 1992, the data sample is defined by overwater pixels from the *F-11* SSM/I meeting the criterion $T_{22V} - T_{19V} < 5$ K, where V indicates vertical polarization. In a tropical or temperate environment for which the signature of water vapor normally gives rise to a large difference between these two channels, this criterion is only fulfilled for FOVs that are almost entirely filled with precipitation that exceeds about 5 mm h^{-1}. By further restricting the sample to contiguous groups of no less than 50 pixels satisfying the above criterion, it becomes likely that most of these pixels represent rainfall that is not only heavy but spatially very extensive and thus, presumably, comparatively uniform and free of strong 3D structure within each FOV. These characteristics are desirable for the purpose of comparing observed and theoretically predicted multichannel signatures of heavy rainfall.

The final sample consisted of a total of 3203 pixels representing 46 contiguous clusters of 50 or more pixels

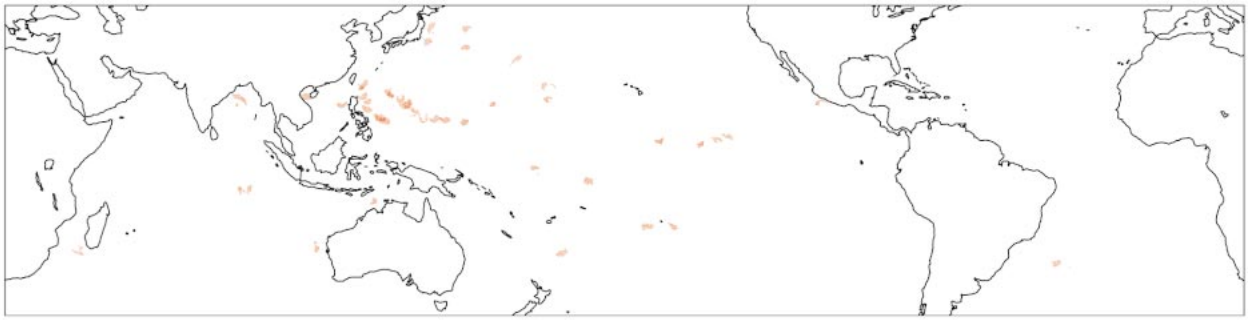

FIG. 2. Locations (in red) of rain events in study sample.

(Fig. 2). That 9 months of global SSM/I data yielded a sample this small, representing an estimated 0.03% of the total overwater pixels affected by precipitation in some form, is an indication of how rarely heavy precipitation is found over such a large contiguous area. An unanticipated by-product of the stringent selection criteria was that most of the 46 cases were found to be associated with organized tropical cyclones, many possessing an identifiable ''eye'' in the SSM/I imagery (Fig. 3). All results presented in this paper are therefore applicable primarily to this type of precipitation.

Figure 4 depicts scatterplots of the complete dataset for selected combinations of channels and channel differences. In these plots, the channel difference $T_{22V} - T_{19V}$ is taken as a crude measure of the optical density of the rain cloud, because, for increasing opacity, differential emission due to water vapor, which normally gives rise to a large positive difference, is increasingly masked by differential emission/extinction of opposite sign due to hydrometeors. The upper limit of 5 K is, of course, a reflection of the selection criteria. The lower limit of approximately -5 K, on the other hand, is determined by the optical properties of the most heavily raining scenes in the sample.

The polarization difference $T_{19V} - T_{19H}$ at 19.35 GHz gives similar information about cloud opacity, because most of the difference at lower frequencies is due to residual visibility of polarized ocean surface emission through the rain layer. At 37 and 85.5 GHz, the clouds are effectively opaque; hence any residual polarization difference must be due primarily to polarization-dependent scattering and extinction in the rain clouds themselves, due in part to presence of preferentially oriented nonspherical particles. At 37 GHz, the mean residual polarization is 3.3 K; at 85.5 GHz it increases to a mean of 7.6 K, with a few instances as large as 15 K. In a few very rare cases, a negative polarization difference of up to 2 K is observed at 85.5 GHz. No negative polarizations are observed at the lower frequencies; indeed, a positive difference of approximately 1 K probably represents a hard lower bound on the 37-GHz polarization difference.

In the bottom row of scatterplots, the vertical and horizontal polarizations are plotted against each other for each frequency. The interpretation of these plots follows Spencer (1986), Spencer et al. (1989), and Petty (1994a). At 19.35 GHz, the dominant source of brightness temperature variability lies in the more or less lin-

FIG. 3. Same as Fig. 2, but focusing on the region 0°–45°N, 100°–180°E.

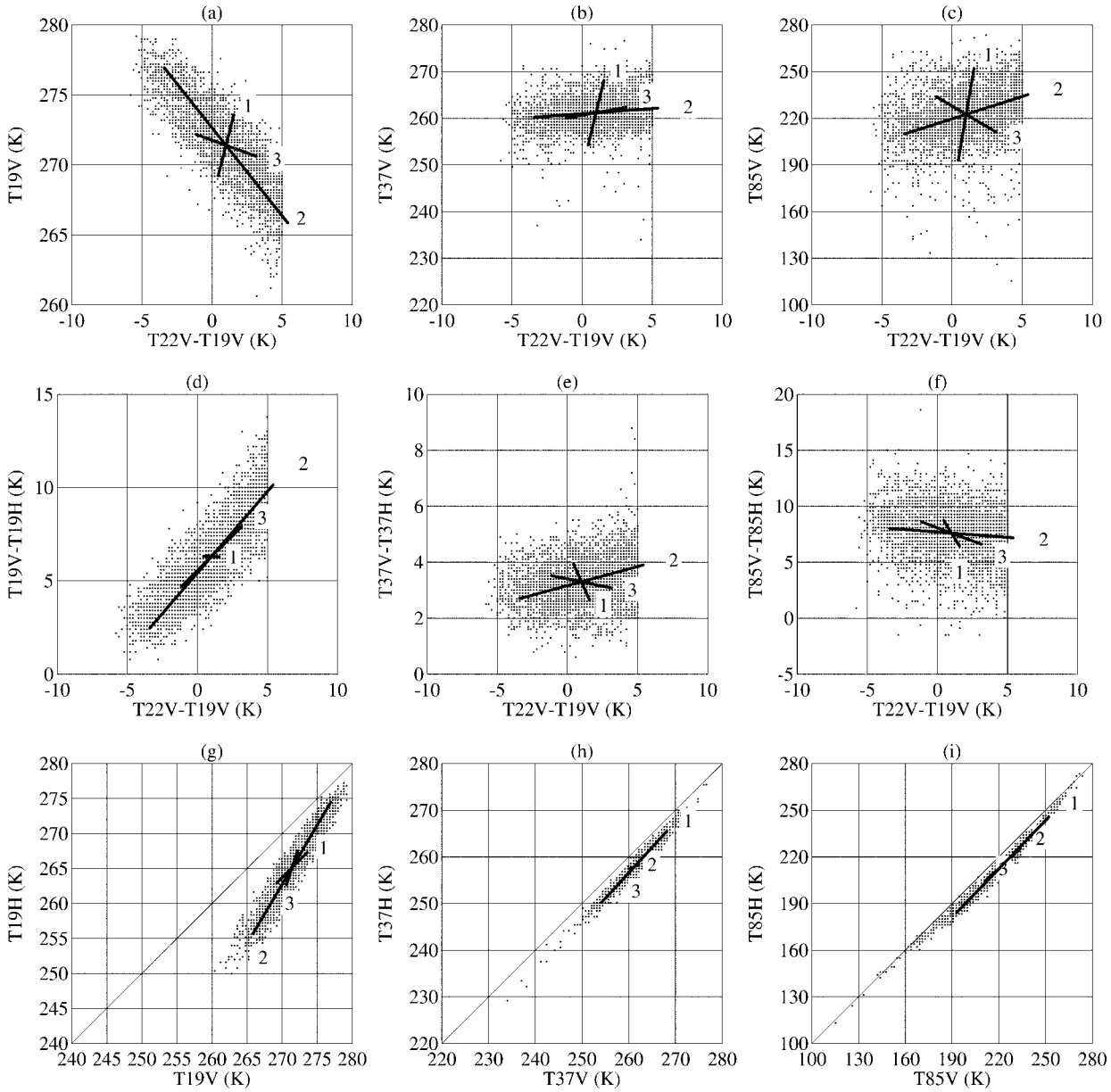

FIG. 4. Observed SSM/I brightness temperatures from widespread, moderate-to-heavy tropical rainfall: (a)–(c) vertically polarized brightness temperatures vs $T_{22V} - T_{19V}$; (d)–(f) polarization differences $T_V - T_H$ vs $T_{22V} - T_{19V}$; (g)–(i) T_V vs T_H (diagonal line indicates polarization difference of zero). From left to right, columns present results for 19.35, 37, and 85.5 GHz, respectively. In all panels, solid lines represent projections of the first three eigenvectors in Table 1. For clarity, the magnitudes of these vectors have been multiplied by a factor of 2.

ear transition between colder, somewhat polarized scenes in which ocean surface emissivity is still visible and the warm, nearly unpolarized T_B expected from a nearly opaque rain cloud. At this low frequency, there is little unambiguous evidence for scattering by ice or large raindrops, whose signal would be manifested in nearly unpolarized but measurably depressed brightness temperatures relative to the cloud's effective thermodynamic temperature (260–280 K). On the contrary, in the most weakly polarized cases (nearest the diagonal line), which also correspond to the heaviest rainfall, 19.35-GHz brightness temperatures range from approximately 270 to as warm as 277 K. These values are all warmer than any point on the 19-GHz emission curves in Fig. 1, implying that the simple model used to generate those curves (and many models like it) overestimates the importance of scattering by ice in this type of rainfall.

For the two higher frequencies, the role of scattering is much more clearly evident. At 37 GHz, minimum brightness temperatures near 230 K are observed, though only a very small percentage of pixels fall sig-

nificantly below 250 K. Moreover, there is a slight tendency for the average polarization difference to increase with increasing scattering—up to 5 K for the coldest brightness temperatures, as compared with approximately 3 K for the sample mean.

At 85.5 GHz, minimum brightness temperatures tend to fall near 160 K, though approximately 10 pixels are colder still, with a minimum near 115 K. Of interest, most very warm and very cold brightness temperatures tend to be completely unpolarized, whereas intermediate values exhibit a mean polarization difference near 8 K. A similar tendency has also been noted by Heymsfield and Fulton (1994), who suggested that larger polarizations may be due to preferentially oriented snow crystals found in stratiform clouds, as contrasted with the tumbling, irregular graupel particles expected in the more strongly convective clouds that produce strong scattering.

Of particular note for 85.5 GHz are a few pixels with brightness temperatures as warm as 274 K, despite the fairly heavy rain rates implied by the other channels. Inspection of the relevant images in these cases failed to reveal any obvious data errors. It is my interpretation that these correspond to moderate rainfall from clouds lacking a significant ice phase. One must then also postulate an overlying heavy layer of warm, nonprecipitating cloud liquid water, both to mask the expected scattering due to raindrops alone and to support the production (via collision–coalescence) of moderate to heavy rainfall in the first place.

3. Empirical multichannel signatures

a. Principal component analysis

The relative homogeneity, both meteorological and spatial, of the above SSM/I observations of precipitation presents an opportunity to quantify the empirical multichannel signature of nearly pure precipitating scenes under fairly reproducible conditions and without the usual complications of incomplete beam-filling and other extraneous factors. If the statistics of the multichannel brightness temperatures can be summarized in a form that can be directly compared with models, then these results can be used to identify, and possibly to correct, interchannel inconsistencies resulting from inappropriate microphysical or radiative assumptions.

Each SSM/I multichannel observation can be viewed as a vector **T** in seven-dimensional channel space. The complete brightness temperature dataset describes a cloud of such points. To first order, the cloud resembles a hyperellipsoid. The centroid of the ellipsoid is the vector mean of the observations. The size, shape, and orientation of the ellipsoid are then described by the 7 $\times$ 7 covariance matrix. Because each channel has a nonzero response to certain properties of the scene being viewed, changes in those properties give rise to highly correlated changes in all channels simultaneously. Physical information is thus spread out over several channels, and no single channel is uniquely identified with one particular physical signal.

If one or more channels happened to be linearly dependent on the remaining channels, then the hyperellipsoid would collapse to a lower-dimensional volume, indicating that the seven-channel microwave observations have fewer than seven real degrees of freedom, a finding that would have important implications for the retrievable information content of the observations. This kind of degeneracy unfortunately cannot be readily detected by inspection of the raw covariance matrix or of 2D scatterplots of various pairs of channels.

A common technique for identifying and characterizing the underlying lower-order dimensionality of a high-dimensional datasets is principal component analysis (PCA), which entails the computation of the eigenvectors and eigenvalues of the covariance matrix. For problems like the current one, this procedure has the following benefits.

1) The eigenvectors indicate the orientation of the principal axes of the covariance ellipsoid in channel space and thus define a rotated coordinate system in which all seven variables describing an observation vector are both linearly independent (orthogonal in channel space) and statistically uncorrelated.
2) The eigenvalues give the variance of the dataset along each of the new coordinate axes. The eigenvector associated with the largest eigenvalue describes the mode of maximum joint variability between channels. Once the eigenvector/eigenvalue decomposition of a covariance matrix is determined, each original observation may be expressed as a linear combination of the eigenvectors, where the linear coefficients (principal components) are obtained by taking the scalar product of the observation vector and the respective eigenvector.
3) If the same linear decomposition is applied to simulated data from a radiative transfer model, then the occurrence of unexpectedly large values of lower-order principal components may reveal shortcomings in the microphysical or microwave optical assumptions in the model.
4) It may prove possible to interpret each eigenvector in terms of a specific mode of microphysical variability in rain clouds. If so, then because each principal component is statistically uncorrelated with the others, the physical variability responsible for multichannel T_B variability might, to first order, be understood in terms of a linear superposition of several quasi-independent modes of physical variability.

The remainder of this paper describes the results of PCA applied to the study sample and suggests qualitative physical interpretations. Some minor embellishments of conventional PCA will be noted as they arise.

TABLE 1. Statistical properties of the SSM/I pixels in this study.

Channel	$\langle T_B \rangle$ (K)	σ (K)	Eigenvectors of correlation matrix converted to physical units and normalized to unit variance						
			$\hat{\mathbf{E}}_1$	$\hat{\mathbf{E}}_2$	$\hat{\mathbf{E}}_3$	$\hat{\mathbf{E}}_4$	$\hat{\mathbf{E}}_5$	$\hat{\mathbf{E}}_6$	$\hat{\mathbf{E}}_7$
T_{19V}	271.4	3.0	1.09	−2.77	0.39	0.03	0.35	0.02	−0.01
T_{19H}	265.1	5.0	1.10	−4.69	1.19	0.25	−0.52	−0.06	0.03
T_{22V}	272.4	1.7	1.37	−0.57	−0.68	−0.45	−0.04	0.00	0.00
T_{37V}	261.2	3.6	3.46	0.48	−0.57	0.62	0.04	−0.32	0.05
T_{37H}	257.9	3.9	3.78	0.18	−0.68	0.79	−0.06	0.33	−0.05
T_{85V}	222.5	17.1	14.77	6.32	5.70	−1.47	−0.09	−0.32	−0.92
T_{85H}	214.9	17.5	15.34	6.53	5.20	−1.68	0.13	0.47	0.95
			Variance explained in correlation matrix						
			59.7%	30.4%	7.0%	2.2%	0.4%	0.2%	0.1%
			Cumulative variance explained in correlation matrix						
			59.7%	90.1%	97.1%	99.3%	99.7%	99.9%	100%

b. Application to the study sample

Means and standard deviations σ were computed separately for each of the seven SSM/I channels, and these were used to scale each channel's brightness temperatures to zero mean and unit variance. The 7×7 correlation matrix was then computed, from which seven eigenvectors and the corresponding eigenvalues were determined.

The use here of the correlation matrix rather than the covariance matrix ensures that the results indicate the relative importance of the various modes of brightness temperature variability in terms of information content rather than in terms of the absolute magnitude of the brightness temperature variation. Otherwise, a single environmental variable that gave rise to unusually large brightness temperature fluctuations in one or more channels could dominate the total variance of the sample and obscure physically significant joint variations of small absolute magnitude.

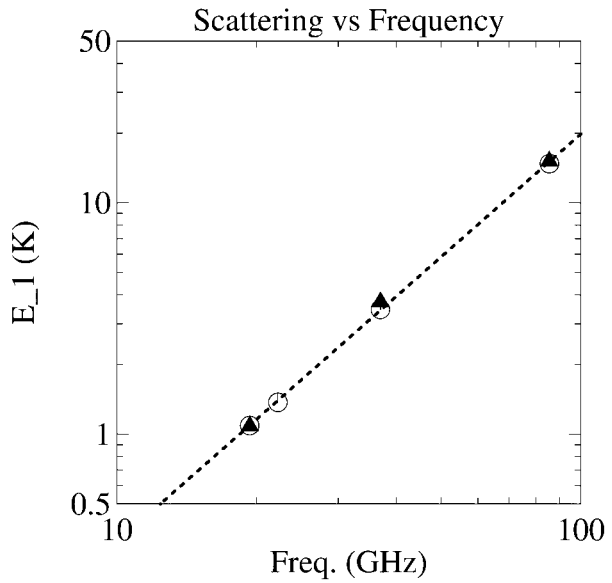

FIG. 5. Elements of first eigenvector $\hat{\mathbf{E}}_1$ plotted vs frequency. Circles represent vertically polarized channels; solid triangles represent horizontally polarized channels. Dashed line depicts the power law $y = 5.88 \times 10^{-3} \nu^{1.764}$.

The elements of the resulting eigenvectors were remultiplied by the standard deviations in the second column of Table 1 so as to yield physical units (K) and then were renormalized so that the magnitude of the eigenvector elements gives the channel brightness temperature standard deviation associated with that eigenvector (i.e., summing the eigenvector elements in quadrature for a given channel yields the total standard deviation for that channel). Thus, the renormalized eigenvectors describe the characteristic direction *and* magnitude (in brightness channel space) of the component of variability in the observations associated with that eigenvector.

The complete set of rescaled eigenvectors is given in Table 1. Projections of the first three eigenvectors (multiplied by 2) are superimposed on the scatterplots described previously (Fig. 4).

c. Qualitative interpretation

The first eigenvector $\hat{\mathbf{E}}_1$, explaining 60% of the total variance in the correlation matrix, is essentially unpolarized and its elements increase monotonically with frequency. At 85.5 GHz, this eigenvector contributes variations of typically 17 K in the observed brightness temperature. Because the rain clouds observed in this sample are known to be optically thick at this frequency, there is little doubt that the first eigenvector is associated with variations in the so-called scattering signature of ice particles in the upper layers of the rain clouds. Figure 5 shows that the elements of this eigenvector describe a nearly perfect straight line in a log–log plot versus frequency ν, implying an accurate power-law relationship proportional to $\nu^{1.76}$. This spectral dependence turns out to constrain strongly the effective mean sizes of the

TABLE 2. Qualitative interpretation of eigenvectors.

$\hat{\mathbf{E}}_1$	Variations in overall intensity of scattering, uncorrelated with near-surface precipitation
$\hat{\mathbf{E}}_2$	Intensity of near-surface precipitation
$\hat{\mathbf{E}}_3$	Anomalous 85.5-GHz scattering with respect to near-surface precipitation
$\hat{\mathbf{E}}_4$	Anomalous scattering at 85.5 GHz with respect to scattering at 37 GHz
$\hat{\mathbf{E}}_5$	Anomalous 19-GHz polarization with respect to 19-GHz T_B
$\hat{\mathbf{E}}_6$	Oriented scatterers affecting both 37- and 85.5-GHz polarization
$\hat{\mathbf{E}}_7$	Oriented scatterers affecting 85.5-GHz polarization only

ice particles responsible for the scattering. The quantitative interpretation of the current empirical results is the subject of Part III of this study (PG01).

The second eigenvector $\hat{\mathbf{E}}_2$ contains most of the variability in the 19-GHz polarization difference and in $T_{22\mathrm{V}} - T_{19\mathrm{V}}$. It is, therefore, apparently a measure of the residual FOV-averaged transmittance at the lowest frequencies. Because this transmittance is most strongly influenced by rain intensity below the freezing level (in the case of uniform rain layer depth and complete FOV-filling), we tentatively interpret this eigenvector as an indicator of the surface rain intensity. Model simulations described in a companion paper (PG01) corroborate this interpretation. Although a significant component of unpolarized variability in the 85.5-GHz channels is associated with $\hat{\mathbf{E}}_2$, the latter's contribution is significantly smaller than that due to $\hat{\mathbf{E}}_1$, suggesting that 85.5-GHz scattering is a poor proxy for surface rain rate in the current dataset.

The third eigenvector $\hat{\mathbf{E}}_3$ is typically responsible for brightness temperature variations of about less than 1 K for all channels except at 85.5 GHz, where it adds another approximately 5 K of variability. Eigenvector $\hat{\mathbf{E}}_3$ therefore represents significant variations in brightness temperature at this frequency that are uncorrelated with variations at lower frequencies.

The fourth through seventh eigenvectors contribute relatively little to the total brightness temperature variability. Also, because they are constrained to be orthogonal to each other and to the three most significant eigenvectors, there is no reason to expect that they will have unambiguous physical interpretations. Nevertheless, their qualitative roles in the multichannel signature of the rain events analyzed here are summarized in Table 2.

Together, $\hat{\mathbf{E}}_1$, $\hat{\mathbf{E}}_2$, and $\hat{\mathbf{E}}_3$ explain 97.1% of the total variance in the correlation matrix. It follows that three statistically independent variables are sufficient to explain all but the most subtle multichannel brightness temperature variations in the sample. That is,

$$\mathbf{T} \approx c_1\hat{\mathbf{E}}_1 + c_2\hat{\mathbf{E}}_2 + c_3\hat{\mathbf{E}}_3 + \langle \mathbf{T}_B \rangle, \qquad (1)$$

where the coefficients c_i are uncorrelated and have unit variance and $\langle\ \rangle$ is the observed mean. The ability to describe the joint variability of SSM/I's seven channels in such a concise form (for the type of rainfall represented in the study sample) is important with respect to several of the objectives of this study:

- One may seek to identify specific perturbations of the mean environmental state that are responsible for the T_B variations described by each of the first three eigenvectors. If this proves possible, then the coefficients c_x derived from any given observation vector are rough measures (exact, in the case of a linear response) of the sign and relative magnitude of the corresponding perturbation.
- One may further identify environmental states that are statistically or physically unrealistic (relative to the study sample), to the extent that these lead to brightness temperature variations that are inconsistent with Eq. (1).
- One may identify defects in the forward radiative transfer model itself if, for example, one is unable to find any combination of input parameters that produces brightness temperatures satisfying Eq. (1).

These applications of Eq. (1) will be taken up in the companion papers.

In Fig. 6, the values of the coefficients c_i are plotted as images for a few representative rain events taken from the study sample. These images show several interesting features. First, there is considerable spatial coherence to the values within a given rain event, especially for c_1 and c_2. This coherence suggests that the corresponding eigenvectors are indeed associated with mesoscale (as opposed to pixel scale) properties of the rain clouds and that the rain-cloud properties are indeed fairly uniform within individual pixels, as required for a reasonably unambiguous physical interpretation to be possible.

Second, there is little correlation between the values of the coefficients c_i, either within individual rain events or when considering variations between events. This confirms that each principal component is highlighting a different physical characteristic of the rain cloud. The quantitative physical interpretation of the different principal components is taken up in a companion paper (PG01).

Third, there are cases for which the overall value of one of the coefficients is anomalously low or high for an entire rain event while the other coefficents may fall in their normal range. From this result, I conclude that the microphysical properties responsible for the coefficients in question may be governed in part by the larger-scale environment or perhaps by the point that the entire rain event has reached in its overall life cycle.

4. Conclusions

This paper provides the first concise statistical characterization of cloud-top multichannel SSM/I radiances in relatively heavy, horizontally extensive rainfall over the tropical oceans. The large majority of cases in the study sample are apparently associated with widespread heavy rain in tropical cyclones. The required spatial

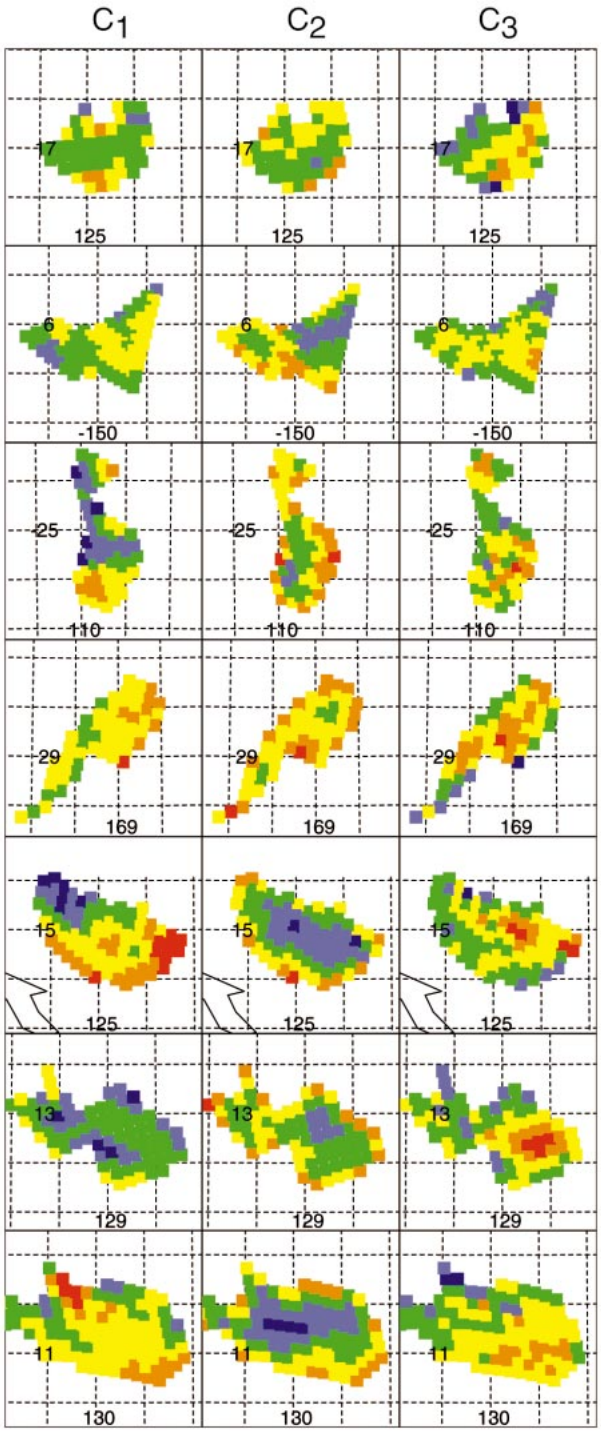

FIG. 6. Examples of principal component decompositions of seven actual rain events in the study sample, based on Eq. (1). Only the first three principal components are plotted. The color scale encompasses values of c_i ranging from -2 (dark blue) to $+2$ (red). Center lat and long are indicated for each subfigure.

extent of the rainfall reduces the influence of incomplete beam-filling on the observed brightness temperatures, and the relatively high optical thickness of the rain events reduces the influence of the ocean surface. Both characteristics are highly desirable when the objective is to isolate the influence of cloud microphysical properties alone based on observed multichannel radiances.

The rain clouds sampled here are presumed to be microphysically similar in many respects to the stratiform tropical clouds observed by McGaughey and Zipser (1996) using an airborne microwave radiometer. That study had the advantage of higher-resolution passive microwave data supplemented by radar and other cloud physical measurements but was limited to only two events, each of comparatively light surface rain rate. The current study has a much larger statistical sample and more microwave channels with which to work (including polarization diversity) but lacks independent measurements of cloud properties. Thus, the information provided by both kinds of studies is complementary. This complementarity can and should be exploited when validating and improving cloud microphysical and microwave optical assumptions in forward models.

Findings of particular note include the following:

- In the study sample, there are instances of relatively heavy near-surface rain rates, as inferred from the lower-frequency channels of SSM/I, associated with 85.5-GHz brightness temperatures as warm as 274 K. These cases are suggestive of rainfall from clouds with relatively warm tops and in which scattering by raindrops alone is masked by heavy cloud liquid water at higher levels.
- In the relatively heavy tropical stratiform rainfall considered in this study, the correlation between the scattering signature by ice at high frequencies, as represented in particular by the first eigenvector $\hat{\mathbf{E}}_1$, and indications of near-surface rain intensity at lower frequencies is weak.
- The eigenvector $\hat{\mathbf{E}}_1$, which contains most of the spectral dependence of scattering-induced brightness temperature depressions due to ice, is remarkably well described by a power-law relationship proportional to $\nu^{1.76}$. This observed spectral dependence of ice scattering is expected to impose a strong constraint on the effective mean sizes of the ice particles responsible for the scattering and can therefore be exploited to improve forward models. Furthermore, this empirical relationship potentially can be used to interpolate or to extrapolate the magnitude of the SSM/I response to scattering to frequencies observed by other microwave sensors.

The quality of any theoretical model for predicting SSM/I brightness temperatures from relatively heavy stratiform tropical rainfall can be gauged in part by its consistency with the simple statistical model given by Eq. (1). In Part II of this study (Petty 2001), a new parametric stratiform cloud model is presented that pro-

vides a foundation for further investigations of the relationship between cloud microphysical properties and microwave radiances. In Part III (PG01), brightness temperature vectors characteristic of the empirical data described herein are physically inverted in order to find model clouds that can explain the mean observed brightness temperatures $\langle \mathbf{T}_B \rangle$ and variations corresponding to $\hat{\mathbf{E}}_1$, $\hat{\mathbf{E}}_2$, and $\hat{\mathbf{E}}_3$.

Once the model has been adjusted empirically to yield observed microwave radiances consistent with Eq. (1) at SSM/I frequencies, the model can act as a physical bridge between the empirical SSM/I brightness temperatures described in this paper and those to be expected at the frequencies and viewing angles of other microwave sensors, such as the Advanced Microwave Sounding Unit, the Tropical Rainfall Measuring Mission (TRMM) Microwave Imager, and the Advanced Microwave Scanning Radiometer.

Acknowledgments. This study was undertaken with support from NASA Grants NAG8-1233 from NASA Marshall Space Flight Center and NAG5-7741 from the TRMM Project Office.

REFERENCES

Aonashi, K., A. Shibata, and G. Liu, 1996: An over-ocean precipitation retrieval using SSM/I multichannel brightness temperatures. *J. Meteor. Soc. Japan,* **74,** 617–637.

Bauer, P., and P. Schluessel, 1993: Rainfall, total water, ice water, and water vapor over sea from polarized microwave simulations and Special Sensor Microwave/Imager data. *J. Geophys. Res.*, **98,** 20 737–20 759.

Evans, K. F., and G. L. Stephens, 1995a: Microwave radiative transfer through clouds composed of realistically shaped ice crystals. Part I: Single scattering properties. *J. Atmos. Sci.*, **52,** 2041–2057.

——, and ——, 1995b: Microwave radiative transfer through clouds composed of realistically shaped ice crystals. Part II: Remote sensing of ice clouds. *J. Atmos. Sci.*, **52,** 2058–2072.

——, J. Turk, J. Wong, and G. L. Stephens, 1995: A Bayesian approach to microwave precipitation profile retrieval. *J. Appl. Meteor.*, **34,** 260–279.

Haferman, J., T. Smith, and W. Krajewski, 1997: A multi-dimensional discrete-ordinates method for polarized radiative transfer. 1. Validation for randomly oriented axisymmetric particles. *J. Quant. Spectrosc. Radiat. Transfer,* **58,** 379–398.

Heymsfield, G. M., and R. Fulton, 1994: Passive microwave and infrared structure of mesoscale convective systems. *Meteor. Atmos. Phys.*, **54,** 123–139.

Hollinger, J. P., J. L. Peirce, and G. A. Poe, 1990: SSM/I instrument evaluation. *IEEE Trans. Geosci. Remote Sens.*, **28,** 781–790.

Kummerow, C., and J. A. Weinman, 1988: Determining microwave brightness temperatures from precipitating, horizontally finite and vertically structured clouds. *J. Geophys. Res.*, **93,** 3720–3728.

——, W. S. Olson, and L. Giglio, 1996: A simplified scheme for obtaining precipitation and vertical hydrometeor profiles from passive microwave sensors. *IEEE Tran. Geosci. Remote Sens.*, **34,** 1213–1232.

Liu, Q., and C. Simmer, 1996: Polarization and intensity in microwave radiative transfer. *Contrib. Atmos. Phys.*, **64,** 535–545.

——, ——, and E. Ruprecht, 1996: 3-D radiation transfer effects of clouds in the microwave spectral range. *J. Geophys. Res.*, **101,** 4289–4298.

Marzano, F., A. Mugnai, N. Pierdicca, E. Smith, J. Turk, and J. Vivekanandan, 1995: Precipitation profile retrieval from airborne microwave radiometers: A case study over ocean during CaPE. *Microwave Radiometry of the Environment,* D. Solimini, Ed., VSP Press, 456–466.

——, ——, G. Panegrossi, N. Pierdicca, E. Smith, and J. Turk, 1999: Bayesian estimation of precipitating cloud parameters from combined measurements of spaceborne microwave radiometer and radar. *IEEE Trans. Geosci. Remote Sens.*, **37,** 596–613.

McGaughey, G., and E. J. Zipser, 1996: Passive microwave observations of the stratiform regions of two tropical oceanic mesoscale convective systems. *J. Appl. Meteor.*, **35,** 1949–1962.

Olson, W. S., 1989: Physical retrieval of rainfall rates over the ocean by multispectral microwave radiometry: Application to tropical cyclones. *J. Geophys. Res.*, **94,** 2267–2280.

Panegrossi, G., and Coauthors, 1998: Use of cloud model microphysics for passive microwave-based precipitation retrieval: Significance of consistency between model and measurement manifolds. *J. Atmos. Sci.*, **55,** 1655–1673.

Petty, G. W., 1994a: Physical retrievals of over-ocean rain rate from multichannel microwave imagery. Part I: Theoretical characteristics of normalized polarization and scattering indices. *Meteor. Atmos. Phys.*, **54,** 79–100.

——, 1994b: Physical retrievals of over-ocean rain rate from multichannel microwave imagery. Part II: Algorithm implementation. *Meteor. Atmos. Phys.*, **54,** 101–121.

——, 2001: Physical and microwave radiative properties of precipitating clouds. Part II: A parametric 1D rain-cloud model for use in microwave radiative transfer simulations. *J. Appl. Meteor.*, **40,** 2115–2129.

Roberti, L., and C. Kummerow, 1999: Monte Carlo calculations of polarized microwave radiation emerging from cloud structures. *J. Geophys. Res.*, **104,** 2093–2104.

——, J. Haferman, and C. Kummerow, 1994: Microwave radiative transfer through horizontally inhomogeneous precipitating clouds. *J. Geophys. Res.*, **99,** 16 707–16 718.

Smith, E. A., X. Xiang, A. Mugnai, and G. J. Tripoli, 1994: Design of an inversion-based precipitation profile retrieval algorithm using an explicit cloud model for initial guess microphysics. *Meteor. Atmos. Phys.*, **54,** 53–78.

Spencer, R. W., 1986: Satellite passive 37-GHz scattering-based method for measuring oceanic rain rates. *J. Climate Appl. Meteor.*, **25,** 754–766.

——, H. M. Goodman, and R. E. Hood, 1989: Precipitation retrieval over land and ocean with the SSM/I: Identification and characteristics of the scattering signal. *J. Atmos. Oceanic Technol.*, **6,** 254–273.

Turk, J., and J. Vivekanandan, 1995: Effects of hydrometeor shape and orientation upon passive microwave brightness temperature measurements. *Microwave Radiometry of the Environment,* D. Solimini, Ed., VSP Press, 187–196.

Wentz, F. J., 1992: Measurement of oceanic wind vector using satellite microwave radiometers. *IEEE Trans. Geosci. Remote Sens.*, **30,** 960–972.

——, and R. W. Spencer, 1998: SSM/I rain retrievals within a unified all-weather ocean algorithm. *J. Atmos. Sci.*, **55,** 1613–1627.

Wilheit, T. T., 1986: Some comments on passive microwave measurement of rain. *Bull. Amer. Meteor. Soc.*, **67,** 1226–1232.

——, A. T. C. Chang, and L. S. Chiu, 1991: Retrieval of monthly rainfall indices from microwave radiometric measurements using probability distribution functions. *J. Atmos. Oceanic Technol.*, **8,** 118–136.

Wu, R., and J. A. Weinman, 1984: Microwave radiances from precipitating clouds containing aspherical ice, combined phase, and liquid hydrometeors. *J. Geophys. Res.*, **89,** 7170–7178.